Influence of Bubble Size on the Foaming Behavior of Molten Slag Containing FeO

WON YEONG SON, SEONG-HOON KEE, and YOUNGJO KANG

To clarify the relationship between bubble sizes and slag foaming behavior, foaming height of molten slag containing FeO was investigated under gas injection with wide range of flow rate. The slag composition was changed considering the addition of direct reduced iron (DRI), and the bubble size was determined at various flow rates using the frequency of bubble formation. The measurement results revealed that the critical value of flow rate exists and at flow rates higher than the critical value, the bubble size tended to increase as the flow rate increases. Because the phenomena of slag foaming are significantly influenced by the bubble size, it is necessary to carefully consider the change in the bubble size in the estimation of the slag foaming index. Moreover, dimensional analysis was used to derive an expression for the slag foaming index considering the bubble size.

I. INTRODUCTION

SLAG foaming phenomena in metallurgical processes have been investigated in the steelmaking process, particularly in the electric arc furnace (EAF) and basic oxygen furnace (BOF) processes. Recently, the EAF steelmaking process has been widely applied owing to its environmental benefits based on low carbon dioxide emissions. Proper utilization of the slag foaming behavior in EAF process has known to be greatly beneficial for energy efficiency and protection of refractories.[1,2] Therefore, it is crucial to optimize of slag foaming phenomena in modern EAF processes, and in-depth understanding about the fundamental features of slag foaming is strongly required.

Bikerman[3,4] suggested a "foaming index" as a quantitative indicator of the foaming behavior of an aqueous solution and verified that this index is solely determined by the properties of the liquid. This foaming index is expressed by Eq. [1]:

$$\Sigma = \frac{\Delta h}{\Delta V_g^s},\qquad [1]$$

where Δh is the change in the height of the slag foam (cm) and ΔV_g^s is the change in superficial gas velocity (cm s^{-1}). The slag foaming behavior at high temperatures has been investigated by several authors.[5–8] Cooper and Kitchener[7] measured foam lifetime in CaO–SiO$_2$–P$_2$O$_5$ system and concluded that foaming is facilitated by a lower CaO/SiO$_2$ ratio, lower temperature, and greater P$_2$O$_5$ content. Swisher and McCabe[8] conducted similar experiments using the CaO–SiO$_2$–Cr$_2$O$_3$ system and reported that the lifetime of the slag foam is significantly increased by the Marangoni effect arising from surface activation by Cr$_2$O$_3$. In this regard, considering the effect of the physical properties on the value of the slag foaming index, various studies focused on the design of mathematical models that take into account certain properties of the slag. Ito and Fruehan[9,10] suggested that the foaming index was correlated with the physical properties which were verified by the elaborated dimensional analysis. Many subsequent authors have also described slag foaming behavior by determining the foaming index and by conducting dimensional analysis.[9–15] As a result of extensive work, the viscosity, surface tension, and density of the slag were deemed to be the most influential factors in the foaming behavior of the molten slag.[10–12,15]

According to Zhang and Fruehan,[14] the physical properties of the gas bubbles in the foam must be considered in dimensional analysis. Although different slag foams may reach the same height, the foams may have the morphologies and the size of the gas bubble cells may be varied across a wide range; hence, lifetimes of the slag foam may differ. The bubbles in the foam can two possible shapes: spherical and polyhedron

WON YEONG SON and YOUNGJO KANG are with the Department of Material Science and Engineering, Dong-A University, 37, Nakdong-daero 550beon-gil, Saha-gu, Pusan 49315, Republic of Korea. Contact e-mail: youngjok@dau.ac.kr SEONG-HOON KEE is with the Department of ICT integrated Ocean Smart Cities Engineering, Dong-A University, 37, Nakdong-daero 550beon-gil, Saha-gu, Pusan 49315, Republic of Korea.

shaped.[16,17] Spherical bubbles are often relatively small, similar to beer foam. Polyhedron-shaped bubbles usually have large bubble cells with polyhedral shapes with very thin liquid lamellae separating them, similar to soap bubble foam. Consequently, the lifetime of slag foam not only depends on its intrinsic physical properties but also on the bubble size. The formation of slag foam in the steelmaking process can be divided into small bubbles generated by chemical reactions and relatively large bubbles by gas injection.[1,14] In addition, the direct reduced iron (DRI) has drawn attention as an alternative raw material for EAF steelmaking. And when DRI is used in the EAF process, the chemical reactions between carbon and FeO in DRI or EAF slag is likely to produce a large number of small bubbles, which may extend the lifetime of the slag foam. Therefore, the various bubble sizes would be expected to affect slag foaming behavior in the steelmaking process:

$$FeO + C(s) = Fe(l) + CO(g),$$

$$FeO + [C] = Fe(l) + CO(g).$$
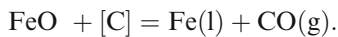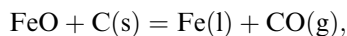
Although it is obvious that slag foaming behavior is considerably affected by bubble size, the effect of the bubble size on the slag foaming behavior has not been sufficiently studied for now. The objective of the present study, therefore, was to measure the foaming index of the slag containing FeO and to investigate the relationship between bubble size and foaming index.

II. EXPERIMENTAL

A. Measurement of the Height of the Slag Foam

The experimental apparatus to measure the height of the slag foam is shown in Figure 1. An electric resistance furnace equipped with $MoSi_2$ heating elements was used with a B-type thermocouple (Pt–30 pct Rh /Pt–6 pct Rh) to establish an isothermal condition.

The slag composition for the measurement was chosen considering the composition change of the EAF slag by DRI addition. Using a typical DRI composition (84 wt pct Fe–9 wt pct FeO–5 wt pct SiO_2–1 wt pct CaO–1 wt pct C), the slag compositions for measurement were estimated as shown in Table I. Each composition listed in Table I corresponds to initial EAF slag (Slag 1), slags in which scrap is replaced with 10 and 20 pct DRI, respectively (Slags 2 and 3), and the basicity (CaO/SiO_2) adjusted slags from Slag 1 and 3, respectively (Slags 4 and 5).

The synthetic slag samples were prepared from mixtures of analytical-grade SiO_2, MgO, MnO, and Al_2O_3. CaO was prepared by heating reagent-grade $CaCO_3$ for 12 hours at 1273 K (1000 °C). The ratio of FeO and $FeO_{1.5}$ in FeO_x was controlled to be approximately 9:1. And FeO was prepared by mixing Fe powder and Fe_2O_3 powder in a constant proportion and heating them to 1373 K in an ultra-high-purity (UHP)
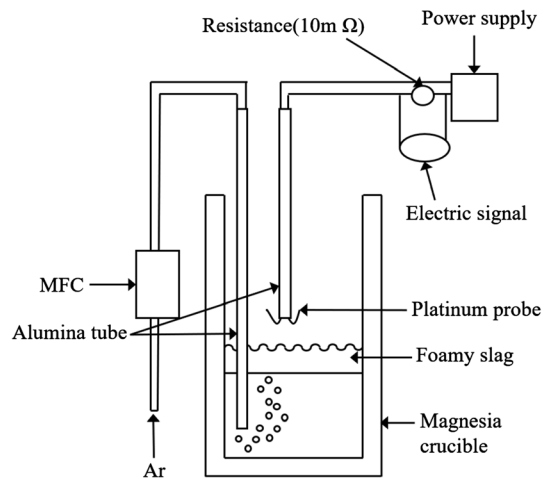

Fig. 1—Schematic diagram of experimental setup for slag foam height measurement.

argon (99.9999 pct purity in terms of volume) atmosphere. The slag was pre-melted using an MgO crucible in an atmosphere of UHP argon to achieve compositional homogenization and volume reduction in the early stage of the experiment. Then, 120 g of the slag, which was preset to be about 40 mm depth in a MgO crucible (I.D. = 40 mm, O.D. = 50 mm, h = 150 mm) was placed in the even temperature zone of a $MoSi_2$ resistance furnace, and the temperature was increased to 1823 K. The flow rate of the UHP argon was controlled to remain constant at 8.33 $cm^3 s^{-1}$ using a mass flow controller. Once target temperature was reached, the gas injection tube was placed on 5 mm above the bottom of the crucible. Injection nozzles with internal diameters of 2 and 3 mm were used. UHP argon gas was introduced through the injection tube at a flow rate of approximately 1.7 to 33.3 $cm^3 s^{-1}$ to form a foam layer. The foam height was defined as the increase in the surface level of the slag relative to the original surface level detected by the electric probe. Pt electrodes, a standard resistor, and DC power supply were designed to detect current change when both ends of the electrodes touched the surface of the slag foam at the same time. The geometric conditions for eliminating the wall effects were identified by Ito and Fruehan,[9] and similar conditions were applied in the present research.

B. Measurement of the Bubble Size of the Slag Foam

The apparatus to measure the bubble frequency in molten slag is schematically shown in Figure 2.

In the similar manner to the foam height measurement, molten slag was prepared in the electric resistance furnace. Slag 3 was chosen for the bubble frequency measurement. With the injection of Ar gas, the bubble frequency in the molten slag was measured. During the measurement of the bubble frequency, an accelerometer was attached to the injection lance and then connected to the oscilloscope to measure the voltage to obtain the frequency of vibration, which is caused by periodic

Table I. Compositions of the Investigated Slags

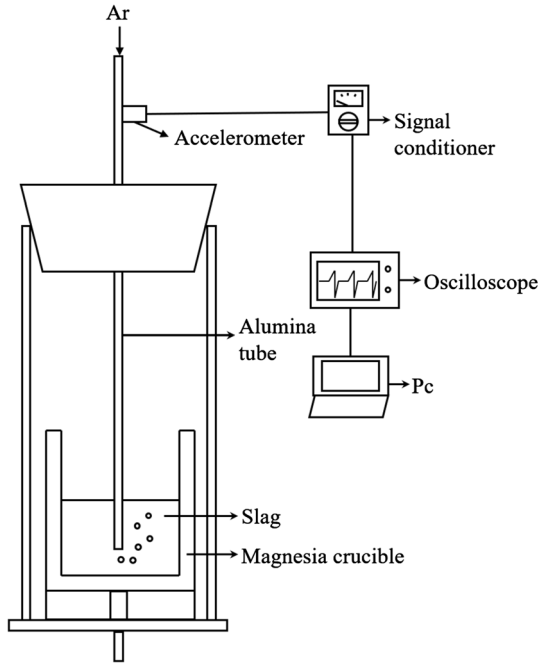| Wt Pct	CaO	SiO$_2$	Al$_2$O$_3$	MgO	FeO$_x$	MnO	CaO/SiO$_2$
Slag 1	23.90	24.14	14.01	7.51	23.44	7.01	0.99
Slag 2	22.76	23.94	13.34	7.15	26.13	6.67	0.95
Slag 3	21.73	23.76	12.74	6.82	28.58	6.37	0.91
Slag 4	23.42	23.65	12.37	6.62	27.74	6.18	0.99
Slag 5	19.52	26.03	14.01	10.00	23.44	7.01	0.75

Fig. 2—Schematic diagram of apparatus for the determination of bubble frequency.

detachment of bubbles from the lance tip. The average bubble size could be estimated from the frequency and the flow rate, as expressed in Eq. [2]:

$$V_b = \frac{Q}{f}, \qquad [2]$$

where V_b is the bubble volume (cm^3), Q is the flow rate (cm^3 s^{-1}), and f is the frequency (s^{-1}). While the injection lances, whose nozzle size was 2, 3 and 4 mm, were used in the measurement, the flow rate was varied in the range 0.33 to 15 cm^3 s^{-1}. To be strict in the above calculation, the Ar gas flow rate should be evaluated at its actual temperature when it is injected into molten slag. Since the gas at room temperature can reach the lance tip in molten slag in less than a second considering the superficial velocity of the gas, it could be presumed that the gas to form a bubble is far from the thermal equilibrium. Therefore, for convenience purposes, the Ar gas flow rate at room temperature was used as the flow rate for bubble formation.

It has been known that bubble size in a fluid can be theoretically defined when the nozzle size is fixed. The relationship between the bubble size and flow rate is separately considered in two regimes depending on the

flow rate: constant volume and constant frequency regimes. The constant volume regime appears when the flow rate through the submerged nozzle is low. The bubble volume can be calculated as the result of a balance between the buoyancy force in the liquid and the surface tension forces constrained by the diameter of the nozzle; hence, the relationship is expressed by Eq. [3][18,19]:

$$V_{bm} = \frac{\pi D_n \sigma}{\rho g}, \qquad [3]$$

where V_{bm} is the bubble volume in the constant volume regime (cm^3), D_n is the diameter of the nozzle (cm), σ is the surface tension (N m^{-1}), ρ is the density (kg m^{-3}), and g is the gravitational acceleration (m s^{-2}). Depending on whether the nozzle material and fluid are wetting or non-wetting, the inner diameter for the diameter of the nozzle should be considered under the wetting condition, and vice versa. On the other hand, the constant frequency regime is valid when the flow rate exceeded a certain limit. Previous studies[20,21] on these phenomena suggested that, during bubble formation, the buoyancy force is balanced against the force required to move the fluid away from the expanding gas–liquid interface. Adopting a classical added mass coefficient of 11/16[22] for the flow rate of the fluid in the vicinity of an accelerating flat plate, the application of Newton's law and further integration with respect to time yields Eq. [4]:

$$V_b = CQ^{1.2} g^{-0.6}, \qquad [4]$$

where V_b is the bubble volume in the constant frequency regime (cm^3), Q is the flow rate (cm^3 s^{-1}), g is gravity (m s^{-2}), and C is a constant. According to Eq. [4], the bubble volume is almost directly proportional to the flow rate. It clearly indicates that the frequency of bubble formation must be practically constant and independent of the gas flow rate. The value of constant C may be the characteristic of a particular fluid and has been reported to be 1.378 for an aqueous system,[20] 1.7 for pig iron,[23] and 1.4 for mercury.[24,25] In this study, it was aimed to determine the size of the slag foam bubbles by using the results of our frequency measurements in these equations.

Table II. Physical Properties and the Foaming Index of the Investigated Slags

	Density* (kg m^{-3})	Surface Tension* (N m^{-1})	Viscosity** (Pa s)	Foaming Index (s)
Slag 1	3175	0.544	0.0455	6.22
Slag 2	3209	0.5464	0.0423	4.90
Slag 3	3241	0.5487	0.0407	4.48
Slag 4	3225	0.5491	0.0394	4.50
Slag 5	3108	0.5379	0.0596	5.03

*Density and surface tension: calculated by the additive method using partial molar volumes[26,27]
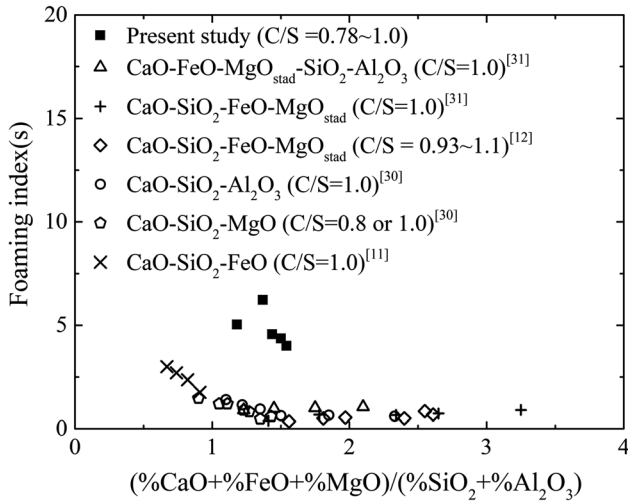**Viscosity: calculated by the Modified Iida's Model[28,29]

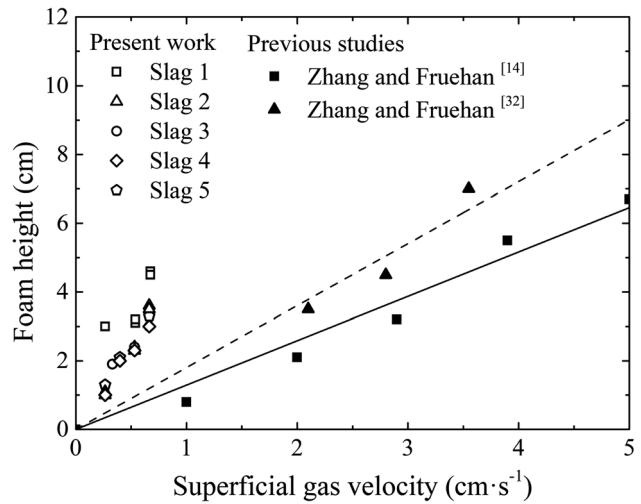Fig. 3—Relationship between slag foaming index and the extended slag basicity.[11,12,30,31]

Fig. 4—Foam height as a function of the superficial gas velocity.[14,32]

III. RESULTS AND DISCUSSION

A. Foaming Index of Slag Containing FeO at Low Flow Rate

The results of the foaming index measurements are summarized with other thermophysical properties in Table II.

The comparison of results of Slag 1, 2, and 3 reveals that the foaming index decreases by the addition of DRI. Slag 1 has the same CaO/SiO_2 as that of Slag 4, but the slag foaming index is higher. This is attributed to the influence of the iron oxides in the DRI. Comparing Slag 3 with Slag 4, the slag foaming index appeared to increase slightly when the CaO/SiO_2 was adjusted to be the same as the initial value after adding the DRI. It is known that the higher CaO/SiO_2 reduces the slag foaming index; however, this case is that the increased concentration of calcium oxide is considered to have increased the slag foaming index owing to the relative dilution of iron oxides. The slag foaming index was found to have a value of 4 to 6 in Table II.

Figure 3 shows the slag foaming index measured in the current work as the function of the extended basicity with those obtained in previous studies.[11,12,30,31] Although the results of the exact same slag system as that in the present study could not be found due to its compositional complexity, the foaming index was confirmed to be rather high compared to the reported values in the previous studies considered the slag system with similar compositions.

As shown in Figure 4, it may be noted that the present flow rate was very low compared with previous research.[14,32] This difference was deemed to have affected the slag foaming behavior. Based on this discrepancy, it could be expected that the flow rate also affects the size of the slag foam bubbles.

B. Bubble Size of Slag Foam in Molten Slag Containing FeO

To determine the frequency of bubble generation, the amplitude of the vibration was measured and recorded by the accelerometer, which was attached to the injection lance. Under the condition in which external sources of vibration were carefully suppressed, the vibrations with markedly large amplitude, as shown in Figure 5, could be regarded to be caused by bubble detachment at the lance tip. The frequency of bubble generation could be obtained from the regularity of the distinct vibrations.

For further verification, the change in the vibration amplitude over time was transformed into another dataset to show how many vibrations were detected at a certain frequency like Figure 6. If the frequency of
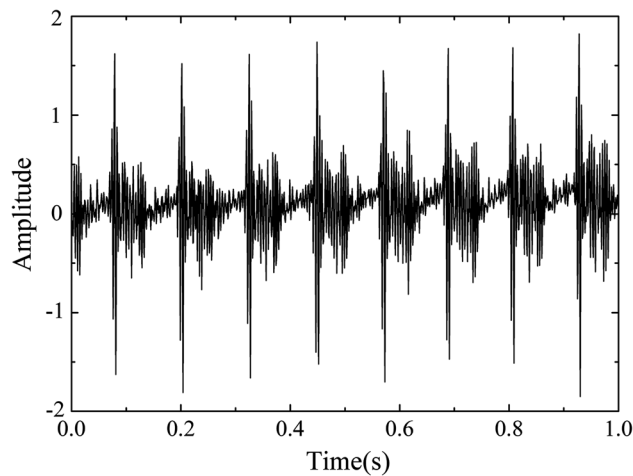
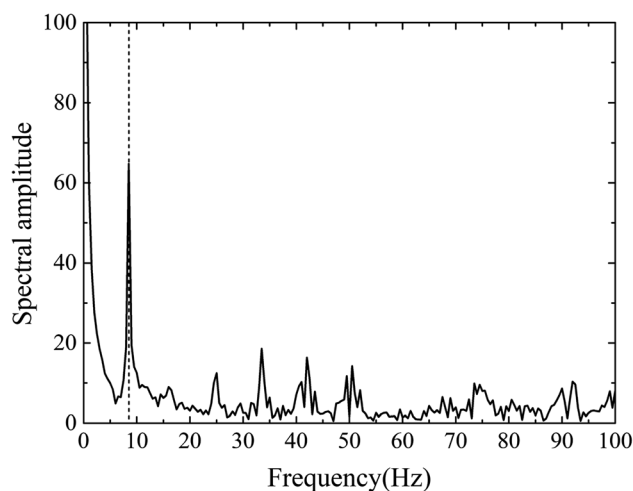Fig. 5—An example of the measurement result for the lance vibrations of during gas injection into molten slag.

Fig. 6—Typical relationship between the spectral amplitude and the vibration frequencies.

Flow Rate (cm³·s⁻¹)	Frequency (Hz)		
	2 mm Nozzle	3 mm Nozzle	4 mm Nozzle
0.33	—	1.60	1.33
0.50	—	2.66	2.00
0.83	7.00	4.00	—
1.00	—	4.00	—
1.33	—	—	5.71
1.67	12.00	7.00	6.66
2.00	—	8.00	7.30
2.33	—	—	7.30
2.50	18.50	—	9.80
3.33	13.50	17.00	12.50
4.17	—	16.00	12.00
5.00	17.50	20.00	13.00
5.83	—	14.00	17.50
6.67	—	16.50	18.50
8.33	18.50	17.00	21.00
10.00	—	17.00	21.50
11.67	—	19.00	25.00
13.33	—	19.50	21.00
14.83	—	19.00	20.50
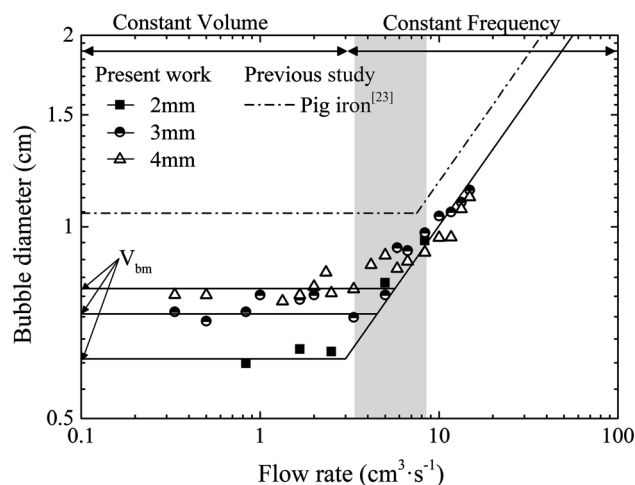
Fig. 7—Bubble diameter as a function of the flow rate in molten slag containing FeO and pig iron.[23]

main vibrations is correctly chosen, its spectral amplitude should be also clearly distinguished. The results of the frequency measurement are listed in Table III.

The bubble size could be further estimated from the frequency of bubble formation and Eq. [2], assuming that all bubbles are spherical. Here, the bubble size stands for that at the moment, when the bubble leaves the lance tip and subsequent changes in the size during bubbles' floatation were not considered for convenience in the present study. The present result of bubble size estimation is plotted in Figure 7.

The bubble diameter V_{bm} in the constant volume region could be calculated to be 0.59, 0.68, and 0.74 cm, respectively, for each nozzle diameter, using Eq. [3]. However, the measured values turned out to be 0.62, 0.73, and 0.8 cm for each nozzle diameter, which are slightly larger than the theoretical values. According to Davidson and Schuler,[20] if the nozzle tip of injection lance is positioned downward, the buoyancy force becomes more significant compared to other forces; consequently, the bubble size might be overestimated. In

spite of the slight difference, reasonable agreement of the measured bubble size with the theoretical value in the constant volume region implies that the present measurement and estimation were adequate. Moreover, the bubble size was estimated to be 0.5 to 1.0 cm at the flow rate of 1.0 to 5.0 cm³·s⁻¹ by the equation proposed by Sano et al.[24,25] Also, Ito and Fruenhan reported that the bubble size at a similarly low flow rate was constant around 1.0 cm.[9] Therefore, the measurement results in the present study could be verified by the comparison with the previous researches.

On the other hand, in the constant frequency region, the y-intercept was determined by introducing a relationship between the volume and the flow rate, as is expressed by Eq. [5]:
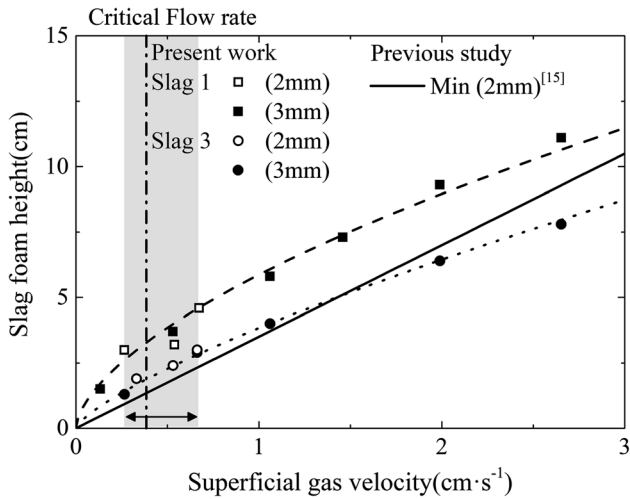
Fig. 8—Foam height of Slags 1 and 3 as a function of the superficial gas velocity.[15]

Fig. 9—Foaming index of Slags 1 and 3 as a function of superficial gas velocity compared with previous results.[14,15]

$$V_b = 1.05 Q^{1.2} g^{-0.6}. \quad [5]$$

The calculated critical flow rates between the constant volume and the constant frequency region for each nozzle diameter were determined to be 3.0, 4.5, and 5.7 $cm^3 \cdot s^{-1}$, respectively. Although the measurement of slag foam height in the present study was carried out under relatively low flow rate, the present flow rate lies around the boundary of the constant volume and the constant frequency region; thus, the bubble size cannot be regarded to be constant. Nonetheless, the bubble size in the present study is smaller than the previous studies,[14,32] and it can be suggested that the effect of the bubble size on the slag foaming behavior should be properly considered.

C. Effect of Bubble Size on Slag Foam Height

To confirm the effect of the bubble size, the slag foam height was measured at higher flow rate. Figure 8 shows the results of the slag foam height, in comparison with the previous results.[15] The present result of slag foam height of Slag 3 reasonably agrees with the previous result plotted as a straight line in Figure 8.[15] The results showed that the rate of change in the slag foam height gradually decreases as the flow rate increases, which might be caused by the increase of bubble size at the higher flow rate. Hence, it could be presumed that the higher foam height in Figure 4 than the previous values was attributed to the small bubble size at low flow rates in the present study.

As mentioned earlier, at very low flow rate compared to the critical value, the bubble size in the constant volume region is related to the nozzle size. Hence, the slope of the slag foam height against the superficial velocity at the low flow rate appeared to be steeper for smaller nozzle size. Since the lance tip with 2 mm nozzle was severely eroded at higher flow rate than 1 cm s^{-1}, the lance with 3 mm nozzle was used at the high flow rate. Beyond the critical flow rate, the slag foam height
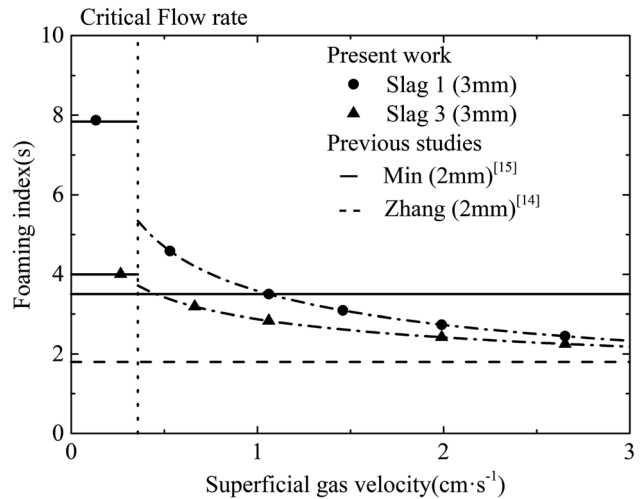
shows similar tendency, no matter whether for 2 or 3 mm nozzle diameter, because the bubble size similarly increases depending on the flow rate in the constant frequency region.

The rate at which the height of the slag foam increased was discovered to decrease as the flow rate increased, so the flow rates should be considered when determining the slag foaming index. Since the slag foaming index is no more constant at a high flow rate, the slag foaming index should be determined at a certain flow rate. An equation to express the relationship between the superficial gas velocity and the slag foam height was derived as Eqs. [6] and [7]:

$$h = 5.87 V_g^{s0.61} \text{ (Slag 1)}, \quad [6]$$

$$h = 3.83 V_g^{s0.75} \text{ (Slag 3)}. \quad [7]$$

The expressions for the slag foaming index considering the flow rate could be obtained by differentiating Eqs. [6] and [7].

$$\Sigma = 3.58 V_g^{s-0.39} \text{ (Slag 1)}, \quad [8]$$

$$\Sigma = 2.88 V_g^{s-0.25} \text{ (Slag 3)}. \quad [9]$$

Figure 9 presents the slag foaming indices for Slags 1 and 3 calculated from Eqs. [8] and [9], along with those determined in previous studies.[14,15]

The results in Figure 9 show that the slag foaming index decreases as the flow rate increases, whereas the slag foaming index in most of the previous researches has been considered to be constant at a relatively higher flow rate (superficial velocity). It is obvious that the flow rate seems to affect the bubble size and the foaming behavior, particularly for small size bubbles in low flow rate conditions, which is important in foaming by

chemical reactions.[33,34] Therefore, precise prediction of the foaming index requires the bubble size to be considered.

D. *Dimensional Analysis*

The foaming index is expected to be related to the physical properties of slags. The viscosity, surface tension, and density are estimated for each composition in Table II. The surface tension and density were calculated using the partial molar values of each oxide,[18,19] whereas the viscosity was calculated using Iida's model.[20,21] The comparison of the various viscosity models[20,21,35–39] indicated that Iida model was the most satisfactory in considering the present slag system. The iron oxide concentration was estimated by assuming that the ratio of hematite to magnetite was constant at 1:9.

Dimensional analysis was carried out to determine the relationship between the foaming index and the slag properties. Subsequent to the earlier dimensional analysis of Ito and Fruehan,[10] the dimensional group was modified to include the effect of the bubble size.[14] The prediction equation by Zhang and Fruehan does not seem to be suitable, because the size of slag foam bubbles and the viscosity of molten slag were relatively small in the present study. Therefore, the appropriate expression for the present slag system should be proposed. The foaming index is assumed to be a function of all the variables and dimensional constants:

$$\Sigma = f(\sigma, \mu, D_b, \rho, g), \qquad [10]$$

where $\Sigma, \sigma, \mu, D_b, \rho, g$ are the foaming index (s), surface tension (N m^{-1}), viscosity (Pa s), bubble diameter (m), density (kg m^{-3}), and gravity (m s^{-2}), respectively. Equation [10] contains six variables and three fundamental dimensions; therefore, three dimensionless groups were to be obtained. Through dimensional analysis, the final forms were obtained as follows:

$$\Pi_1 = \frac{\Sigma \sigma}{\mu D_b}, \qquad [11]$$

$$\Pi_2 = \frac{\rho^2 D_b^3 g}{\mu^2}, \qquad [12]$$

$$\Pi_3 = \frac{\mu^2}{\rho \sigma D_b}. \qquad [13]$$

The dimensionless numbers Π_1, Π_2, and Π_3 were calculated from the foaming index at each flow rate, the bubble size at each flow rate, and the physical properties of the slag. Π_2 has been known to Archimedes number Ar, which corresponds to the ratio of gravitational forces to viscous forces. The dependence of the foaming index on the physical properties and the bubble size of slags can be determined by obtaining the relationship

among these three dimensionless groups. The results of the dimensional analysis on the relationship are shown in Figure 10.

An expression for the linear relationship among three dimensionless numbers in Figure 10 could be obtained as Eq. [14].

$$ln\Pi_1 = -ln\left(\Pi_2^{0.9}\Pi_3^{0.95}\right) + 10.45. \qquad [14]$$

Equation [14] is further converted into the final expression for the slag foaming index as follows:

$$\Sigma = 3950 \frac{\mu^{1.1}}{\rho D_b^{0.95} \sigma^{0.1}}. \qquad [15]$$

Equation [15] also indicates that the viscosity, the bubble size, and the density are more influential to the slag foaming index than the surface tension. Compared with the equation proposed by Zhang and Fruehan,[14] the present slag foaming index was found to be more dependent on the bubble size. However, the coefficient of each physical property is still equivalent to the previous research, and it may imply that the physical properties of molten slag have similar effects on slag foaming.

Figure 11 compares the foam index calculated using Eq. [15] and the measured results. In the comparison, the prediction of slag foaming index shows acceptable agreement with the measurement results in the present study. Some results for low flow rate show less consistency compared to those for high flow rate. Since the relationship between the slag foam height and the flow rate is not sufficiently evident, when the flow rate is very low, the expression for the slag foaming index considering the bubble size seems to be less satisfactory in predicting the slag foaming index at low flow rate.
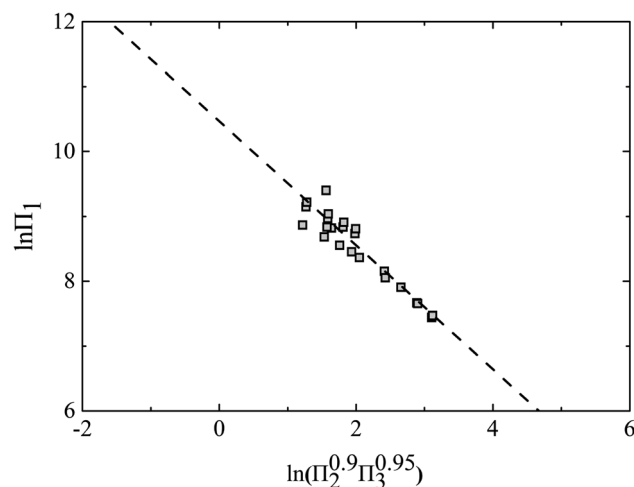

Fig. 10—Result of the dimensional analysis considering the effect of the bubble size.
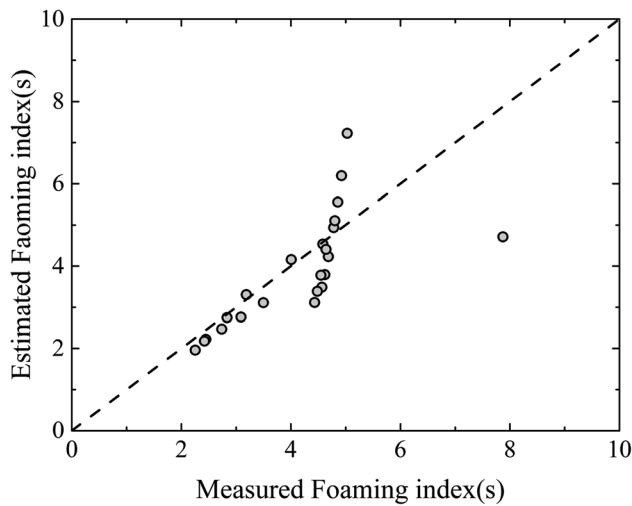
Fig. 11—Comparison between the measured foaming index and that estimated by Eq. [15].

IV. CONCLUSION

The present study investigated the slag foaming behavior in molten slag containing FeO. Owing to the iron oxide contained in the DRI, the slag foaming index tended to decrease as the amount of DRI increased. The slag foaming index was higher than those determined in previous studies, and this was attributed to the relatively low flow rate used in our measurement.

The bubble size measurements confirmed that the constant bubble size was larger than the theoretical value because of larger buoyancy force for the bubble from downward facing nozzle. The bubble size increased as the flow rate increased over the constant frequency regime. Subsequently, the slag foaming index gradually decreased as the flow rate increased. The relationship between flow rate and slag foaming index was derived for molten slag containing FeO.

Considering the effect of the bubble size on the slag foaming behavior, dimensional analysis was conducted to derive an equation to predict the slag foaming index, even when the bubble size changes as the flow rate varies. The slag foaming index derived for the slag containing FeO is expressed as follows:

$$\Sigma = 3950 \frac{\mu^{1.1}}{\rho D_b^{0.95} \sigma^{0.1}}$$

ACKNOWLEDGMENTS

REFERENCES

1. R. Corbari, H. Matsuura, S. Halder, M. Walker, and R.J. Fruehan: *Metall. Mater. Trans. B*, 2009, vol. 40B, pp. 940–48.
2. R.A.M. Almeida, D. Vieira, W.A. Bielefeldt, and A.C.F. Vilela: *Mater. Res.*, 2017, vol. 20, pp. 474–80.
3. J. Bikerman: *Trans. Faraday Soc.*, 1938, vol. 34, pp. 634–38.
4. J. Bikerman: *Ind. Eng. Chem.*, 1965, vol. 57, pp. 81–86.
5. S. Hara and K. Ogino: *ISIJ Int.*, 1992, vol. 32, pp. 81–86.
6. H. Shigeta, M. Ikuta, M. Kitamura, and K. Ogino: *Trans. Iron Steel Inst. Jpn*, 1983, vol. 69, pp. 1152–59.
7. C. Cooper and J. Kitchener: *J. Iron Steel Inst.*, 1959, vol. 193, pp. 48–55.
8. J. Swisher and C. McCabe: *Trans. Metall. Soc. AIME*, 1964, vol. 230, pp. 1669–75.
9. K. Ito and R.J. Fruehan: *Metall. Mater. Trans. B*, 1989, vol. 20B, pp. 509–14.
10. K. Ito and R.J. Fruehan: *Metall. Mater. Trans. B*, 1989, vol. 20B, pp. 515–21.
11. R. Jiang and R.J. Fruehan: *Metall. Mater. Trans. B*, 1991, vol. 22B, pp. 481–89.
12. S.M. Jung and R.J. Fruehan: *ISIJ Int.*, 2000, vol. 40, pp. 348–55.
13. R. Roth, R. Jiang, and R.J. Fruehan: *Ironmak. Steelmak.*, 1992, vol. 19, pp. 55–63.
14. Y. Zhang and R.J. Fruehan: *Metall. Mater. Trans. B*, 1995, vol. 26B, pp. 803–12.
15. H.S. Kim, D.J. Min, and J.H. Park: *ISIJ Int.*, 2001, vol. 41, pp. 317–24.
16. E. Manegold: *Schaum*, Chemie und Technik Verlagsgesellschaft, Heidelberg, 1953.
17. S. Ross and I.D. Morrison: *Colloidal Systems and Interfaces*, Wiley, New York, 1988, p. 294.
18. R.J. Benzing and J.E. Myers: *Ind. Eng. Chem.*, 1995, vol. 47, pp. 2087–90.
19. T. Tadaki and S. Maeda: *Kagaku Kogaku (Abr. Ed.)*, 1963, vol. 1, pp. 55–60.
20. J.F. Davidson and B.O.G. Schuler: *Trans. Inst. Chem. Eng.*, 1960, vol. 38, pp. 335–42.
21. R. Kumar and N.R. Kuloor: *Chem. Technol.*, 1967, vol. 19, p. 733.
22. L.M. Milne Thomson: *Theoretical Hydrodynamics*, 3rd ed., Macmillan and Co. Ltd., London, 1955.
23. G.A. Irons and R.I.L. Guthrie: *Metall. Trans. B*, 1978, vol. 9B, pp. 101–10.
24. M. Sano and K. Mori: *Trans. JIM*, 1976, vol. 17, pp. 344–52.
25. M. Sano, Y. Fujita, and K. Mori: *Metall. Trans. B*, 1976, vol. 7B, pp. 300–01.
26. K.C. Mills and B.J. Keene: *Int. Mater. Rev.*, 1987, vol. 32, pp. 1–120.
27. K. Mills: *The Estimation of Slag Properties, Southern African Pyrometallurgy 2011*, Misty Hills Conference Centre, South Africa, 2011, pp. 1–52.
28. T. Iida, H. Sakai, Y. Kita, and K. Shigeno: *ISIJ Int.*, 2000, vol. 40, pp. 110–14.
29. S. Sukenaga, T. Nagahisa, Y. Gonda, N. Saito, J. Nakashima, and K. Nakashima: *Tetsu-to-Hagané*, 2010, vol. 96, pp. 469–74.
30. Y. Park and D.J. Min: *Metall. Mater. Trans. B*, 2018, vol. 49B, pp. 1709–18.
31. Y. Park and D.J. Min: *Metall. Mater. Trans. B*, 2017, vol. 48B, pp. 3038–46.
32. Y. Zhang and R.J. Fruehan: *Metall. Mater. Trans. B*, 1995, vol. 26B, pp. 1088–91.
33. J. Martinsson, B. Glaser, and D. Sichen: *Ironmak. Steelmak.*, 2019, vol. 46, pp. 777–81.
34. K. Gu, N. Dogan, and K.S. Coley: *Metall. Mater. Trans. B*, 2017, vol. 48B, pp. 2343–53.

35. Q. Shu, L. Wang, and K.C. Chou: *J. Min. Metall. Sect. B*, 2014, vol. 50B, pp. 139–44.
36. Q.F. Shu, X.J. Hu, B.J. Yan, J.Y. Zhang, and K.-C. Chou: *Ironmak. Steelmak.*, 2010, vol. 37, pp. 387–91.
37. G. Urbain, F. Cambier, M. Deletter, and M.R. Anseau: *Trans. J. Br. Ceram. Soc.*, 1981, vol. 80, pp. 139–41.
38. G. Urbain: *Steel Res. Int.*, 1987, vol. 58, pp. 111–16.
39. P.V. Riboud, Y. Roux, L.-D. Lucas, and H. Gaye: *Fachber. Hüttenprax Metallweiterverarb*, 1981, vol. 19, pp. 859–69.